

Coarsening dynamics of falling-film solitary waves

H.-C. Chang,* E. A. Demekhin,† E. Kalaidin,† and Y. Ye

Department of Chemical Engineering, University of Notre Dame, Notre Dame, Indiana 46556

(Received 7 March 1996)

Because interfacial wave dynamics on a falling film involves quasisteady localized solitary pulses, its complex spatiotemporal dynamics exhibits certain generic features and scalings. We construct a statistical theory for such dynamics from our earlier theory for binary pulse interaction [*Physica D* **63**, 299 (1993); *Phys. Rev. Lett.* **75**, 1747 (1995); *J. Fluid Mech.* **294**, 123 (1995)]. The theory shows that the average pulse separation increases linearly downstream from the inlet with a universal slope and that the average pulse velocity increases with a generic power of $2/7$. Prediction for the final equilibrium separation is also offered by the theory. The coarsening features are driven by an irreversible coalescence of the pulses whose local dynamics can be renormalized via an affine transformation due to the scale invariance of the localized pulses. The generic scalings for the dynamics arise from the affine transformation and are favorably compared to numerical simulation and experimental data. [S1063-651X(96)01508-5]

PACS number(s): 47.20.Ky, 47.35.+i, 47.11.+j, 47.20.Ma

I. INTRODUCTION

Open-flow extended-domain systems, such as the falling film, are often “convectively unstable” such that inlet noise is convected into the flow channel and triggers complex spatio-temporal behavior within the otherwise noise-free domains [1,2]. As a result, simulations with low Reynolds number and weakly nonlinear models such as the Kuramoto-Sivashinsky (KS) equation yield such highly irregular fluctuations in space and time that the KS equation has become a prototype for spatiotemporal chaos [3]. However, it was shown recently [4–6] that, when dispersion is added to the KS equation, the irregular fluctuations synchronize into pulselike coherent structures and that, while the dynamics is still quite rich, it is far less random than the KS equation. This observation suggests that low-dimensional deterministic dynamical systems can capture the pulse interaction dynamics faithfully. Since dispersion is introduced by inertia at high Reynolds number, this also suggests that high-Reynolds-number films ($10 < R < 300$) can give rise to low-dimensional dynamics dominated by solitary pulses. This was verified numerically [7,9] with a more realistic model of falling film than the KS equation and experimentally by Liu and Gollub [8] for an inclined film. In the snapshot of Fig. 1 from our simulation, such pulses appear at about $x=200$ in the normalized coordinate or $x=22$ cm in actual units for water from the inlet where random noise was introduced. While residual effects of inlet noise can still be felt in the random distribution of the pulses, the dynamics beyond the inception of pulses was observed to be largely deterministic [9].

This pulse-driven deterministic dynamics involves a unique irreversible coalescence (fusion) of a large pulse with a smaller front pulse [8]. Unlike solitons of integrable systems such as the Korteweg–de Vries (KdV) and nonlinear

Schrödinger equations, such irreversible coalescence creates a single larger pulse which does not split into two pulses. The created pulse then coalesces with more smaller pulses in a cascading fashion. However, the larger pulses also decay in amplitude and speed as they approach the slower and smaller front pulses. As a result, the frequency of coalescence decreases gradually until it stops entirely when the pulse separation is so large that the large pulses created from prior coalescence events cannot chase down their front neighbors to precipitate further coalescence. Such cascading coalescence sequences are seen in the world lines of Fig. 1. As the pulses are eliminated by coalescence, the pulse separation increases downstream (the wave texture coarsens) as is evident in Fig. 1. There is a concomitant increase in the average pulse speed, pulse amplitude, and thickness of the substrate layer beneath the pulse as seen in our simulation shown in Fig. 2. A striking feature of the coalescence dynamics is that the pulse separation $\langle l \rangle$ increases linearly downstream before it saturates at an equilibrium value $\langle l \rangle_\infty$. The pulse speed, on the other hand, seems to increase in some fractional power of the downstream distance x . We shall show that both scalings with respect to x are universal for falling-film pulses and obtain estimates for them from first principles. We also note that the local substrate thickness s is much smaller than the unit flat-film thickness at the inlet and gradually increases from pulse inception to an equilibrium value s_∞ , which is about 0.8 for the standard case shown in Fig. 2.

The statistical theory that yields these generic scalings is based on our earlier deterministic theory for how a large pulse interacts with a smaller front neighbor [7]. Due to the localized structure of the pulses and their slow, quasisteady dynamics, the binary interaction exhibits certain scale invariance such that all interactions can be transformed by an affine transformation to a normalized binary interaction problem involving a family of solitary pulses. At every station along the channel there are then, on the average, two distinct members of the pulse family, a small pulse and a large pulse. The latter pulse arises from fusion of two of the former pulses and hence has twice the area. Knowing the relative fraction of these two pulses, their speeds, and the decay rate

*Author to whom correspondence should be addressed.

†Permanent address: Department of Applied Mathematics, Kuban State Technological University, Krasnodar, 3500072, Russia.

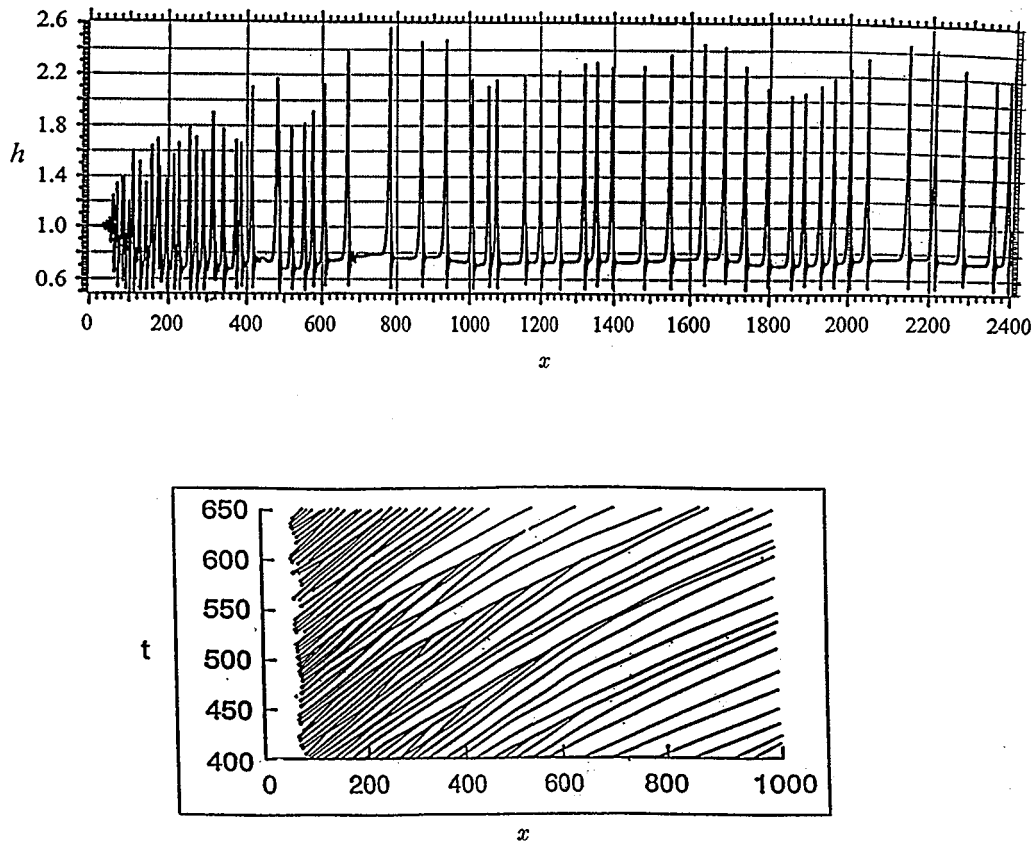


FIG. 1. A snapshot of the wave tracing $h(x,t)$ for $\delta=0.216$. Zero-mean random white noise is introduced to the inlet flow rate while the inlet film thickness is the Nusselt thickness such that $h=1$. Small-amplitude sinusoidal waves precipitate solitary pulses at $x=200$. The pulse separation, amplitude, and substrate thickness increase downstream due to coalescence. Two pulses about to coalesce are seen at $x=375$ and a large pulse results from a coalescence at $x=780$. The coalescence events are also seen in the world lines tracing the pulses below. The pulse speeds are locally constant but gradually accelerate downstream.

of the large pulse, we can hence predict the average coalescence time, the new relative fraction, and, from overall mass balance, the two new members of the pulse family that are generated after the coalescence time. In this manner, an iteration map on the pulse family is established to model the evolution dynamics downstream. The predictions from the theory are in good agreement with our numerical simulation and with some literature data.

II. NORMALIZATION AND SELF-SIMILARITY

Under most realistic conditions at low flow rate but with R in excess of 10, the wave dynamics for a vertically falling film can be described by the averaged equation first derived by Shkadov [10],

$$\frac{\partial q}{\partial t} + \frac{6}{5} \frac{\partial}{\partial x} (q^2/h) - \frac{1}{5\delta} (hh_{xxx} + h - q/h^2) = 0, \quad (1)$$

$$\frac{\partial h}{\partial t} + \frac{\partial q}{\partial x} = 0.$$

This equation is used in the simulations of Figs. 1 and 2. The variable h is the interfacial height and q the average flow rate. The only parameter δ is a modified Reynolds number,

$\delta = R^{11/9}/5\gamma^{1/3}3^{7/9}$, where $\gamma = \sigma\nu^{-4/3}g^{-1/3}/\rho$ is the Kapitza number [12], dependent only on the fluid property, while the Reynolds number $R = \langle u \rangle h_N/\nu$ is defined with respect to the Nusselt flat film with average velocity $\langle u \rangle$ and thickness $h_N = (3\nu\langle u \rangle/g)^{1/2}$. The dimensionless film height h is scaled by h_N and the dimensionless flow rate q by $h_N\langle u \rangle$. The dimensionless downstream coordinate is scaled by κh_N where $\kappa = 3^{-2/9}\gamma^{1/3}R^{-2/9}$.

In our simulation of (1) in Figs. 1 and 2, we use the boundary condition where a zero-mean inlet noise is applied to the Nusselt flat film there. As a result, the time-averaged film thickness and flow rate at the inlet are both unity. However, after the pulses are formed, any given pulse sits on a local substrate layer with local thickness s that is less than unity, as shown in Fig. 2. As the pulse density decreases downstream, s approaches a constant s_∞ close to unity but never quite gets there. Each pulse on a local substrate s moves in a stationary manner with a speed c , as seen from the world lines of Fig. 1. It is the localized width of the pulse structure, which has lost memory of the original thickness h_N and much of the inlet noise, and the stationary speed and shape of the pulses that allow us to develop a rational, largely deterministic theory for these complex dynamics. Transformed to a moving coordinate with speed c , the stationary equation that defines each local pulse then becomes

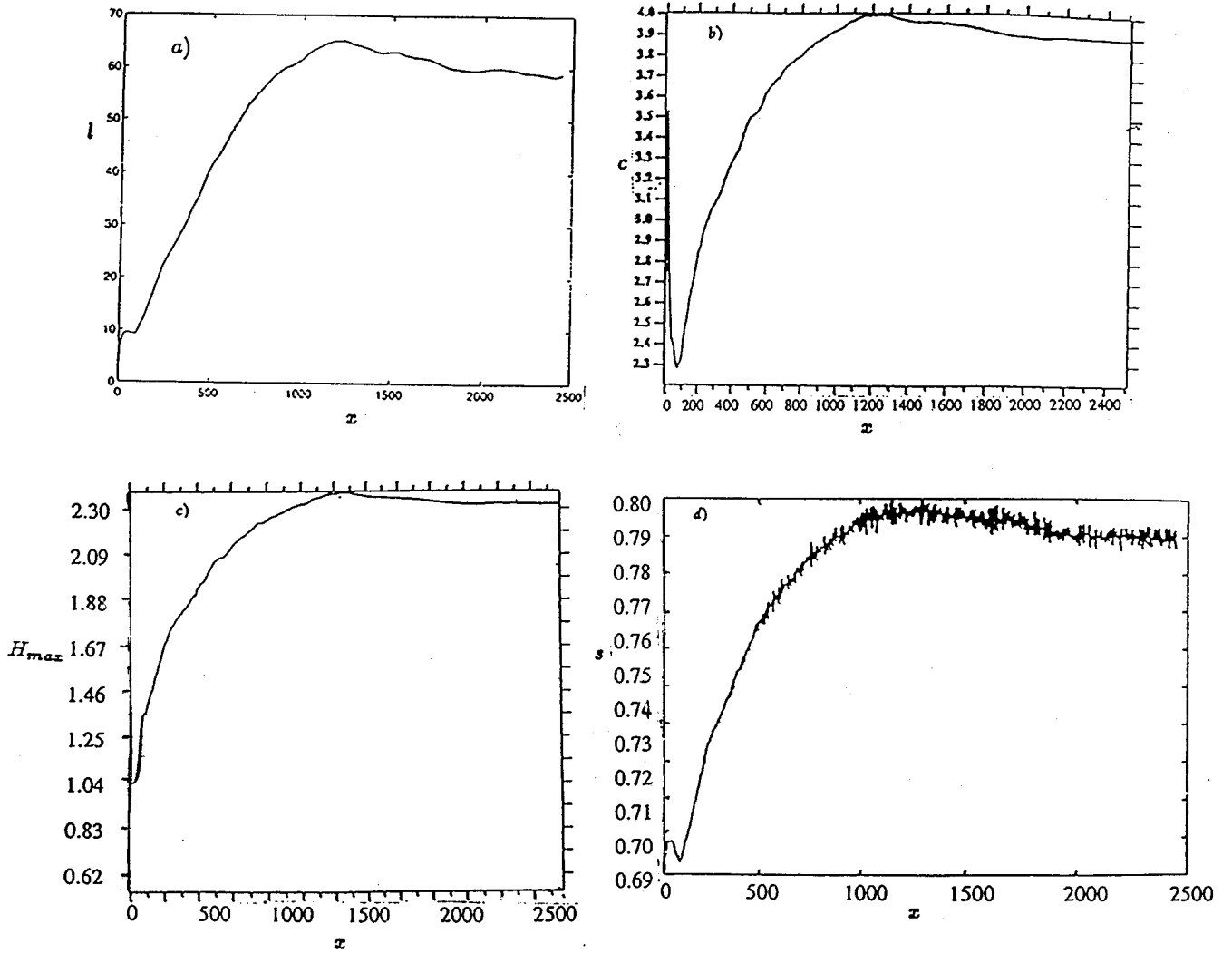


FIG. 2. Time-averaged pulse separation, pulse speed, pulse amplitude, and substrate thickness as a function of downstream position for $\delta=0.216$. Data are taken over 1000 units of time. Pulse inception occurs at $x\sim 200$, beyond which the self-similar dynamics begin.

$$\begin{aligned}
 -cq_x + \frac{6}{5} \frac{\partial}{\partial x} (q^2/h) - \frac{1}{5\delta} (hh_{xxx} + h - q/h^2) &= 0, \\
 -ch_x + q_x &= 0, \\
 h(x \rightarrow \pm\infty) &= s, \\
 q(x \rightarrow \pm\infty) &= s^3.
 \end{aligned}
 \tag{2}$$

yielding the local normalized equation

$$-DQ_x + \frac{6}{5} \frac{\partial}{\partial X} (Q^2/H) - \frac{1}{5\Delta} (HH_{xxx} + H - Q/H^2) = 0,
 \tag{5a}$$

$$-DH + Q = 1 - D,
 \tag{5b}$$

$$H(\pm\infty) = Q(\pm\infty) = 1.
 \tag{6}$$

The substrate flow rate is a factor of s^3 less than the unit flow rate because the parabolic flow profile of a flat film stipulates that its flow rate scales as the cube of the interfacial height.

Since s varies downstream, it is convenient to normalize each substrate thickness to unity. In essence, we choose the local substrate thickness and flow rate to rescale the variables. This then transforms the inlet Reynolds number δ to a local normalized Reynolds number Δ . The corresponding normalizing transformation is a power-law affine transformation involving s :

$$x = s^{1/3}X, \quad h = sH, \quad q = s^3Q, \quad c = s^2D, \quad \delta = s^{-11/3}\Delta,
 \tag{4}$$

The self-similarity allows power-law type scalings in s to eliminate s from (2). We note that while the local Reynolds number Δ is smaller than δ (the inlet Reynolds number), the locally normalized speed D , flow rate Q , and height H all increased because a thinner substrate layer with a smaller flow rate is now used as the reference. The subscript denotes the derivative in Eq. (5a). The fact that every pulse in Fig. 1 with a different s can be normalized to (5) and (6) is because their localized structure stipulates that a flat-film substrate exists locally and there is hence an absence of a specified length scale in the x direction. This allows the affine group transformation parametrized by the substrate thickness s . If, for example, the waves were periodic with a

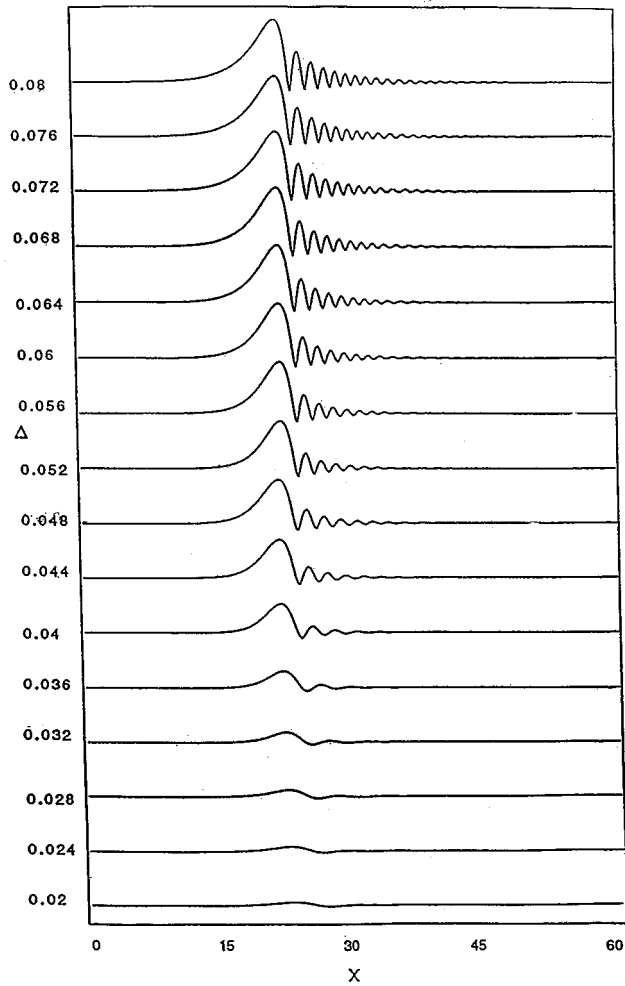


FIG. 3. Normalized solitary pulse family with increasing pulse amplitude as Δ increases. All pulses have unit substrate thickness.

known wavelength, the transformation $x = s^{1/3}X$ would not have been compatible. This existence of self-similarity is quite common for problems in an unbounded domain with no specified length scales. Although (4) has been applied to the averaged equation, similar affine transformations in powers of s exist for solitary waves of the Navier-Stokes equation.

The advantage of this local normalization is that the three parameters c , δ , and s of (2) and (3) are transformed to two parameters Δ and D . The construction of the pulse solution then corresponds to the determination of the nonlinear eigenvalue D as a function of Δ . The construction of this one-parameter family was carried out in [11] and we reproduce the constructed pulse family in Fig. 3 as well as its speed D , area above the substrate $A = \int_{-\infty}^{\infty} (H - 1) dX$, and maximum amplitude H_{\max} in Fig. 4. In Fig. 5, we show that the time-averaged pulse speed from our simulation of Fig. 1, scaled by the time-averaged local average substrate thickness according to (4), falls on the $D(\Delta)$ curve for the speed of the solitary pulse family. This indicates that, while the separation between the pulses is quite random with a broad distribution, each pulse is a quasisteady solitary pulse, and the distribution in the pulse speed is quite narrow at every station, such that the local average pulse is still described by $D(\Delta)$. In the next section, we shall show that there is an intermittent coalescence event, whose frequency is lower than the average pulse frequency, that creates larger pulses. As a result, there are two types of pulses at every station—a small pulse and a large (excited) pulse. However, we shall also show that, due to the linearity of $A(\Delta)$ and the constant asymptote of $D(\Delta)$ at a relatively large Δ , the average speed still belongs to $D(\Delta)$ of the solitary pulse family. Hence, *all* time-averaged pulses at every station belong to the one-parameter pulse family in Fig. 3 after normalization by (4).

We further support this theory by recording the pulse speed and separation distribution of our simulation as shown

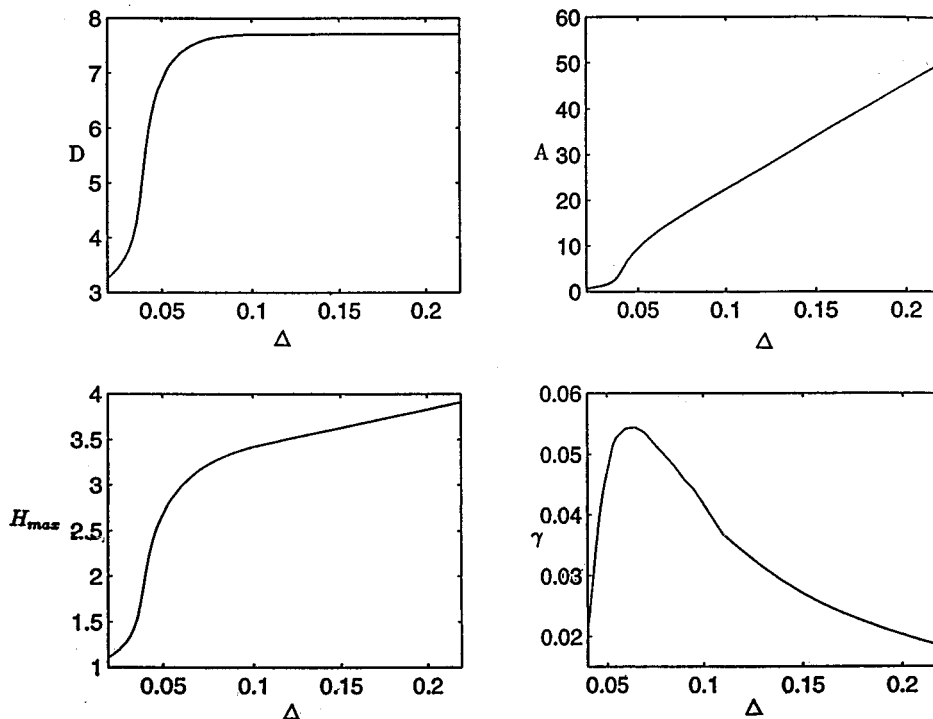


FIG. 4. Speed, area, amplitude, and decay coefficient of the normalized pulse family.

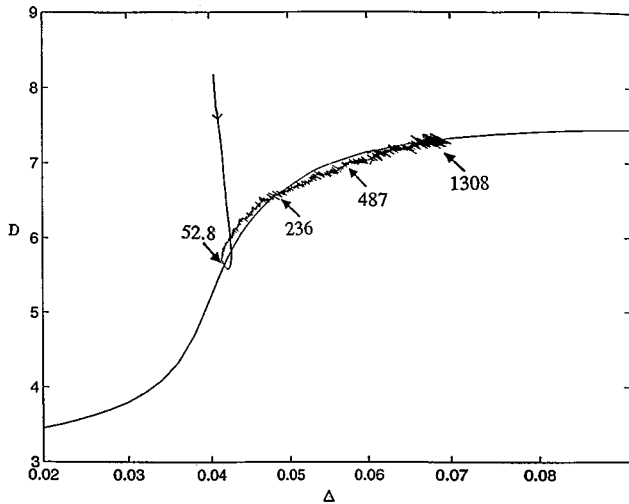


FIG. 5. The normalized speed D and Reynolds number Δ at every station at the indicated x location from the time-averaged data of Fig. 2 plotted against the pulse speed of the normalized family. Quasisteady evolution along the family is clear after pulse inception at $x=200$.

in Fig. 6. While the separation distribution clearly broadens after pulse inception, the speed distribution actually narrows downstream. Although the larger pulses travel faster, their speed is close to the smaller pulse and it is continually decaying towards the latter speed. Consequently, the recording sees a continuous but small band of speeds for these pulses ranging from the speed of the small pulse to the highest speed, corresponding to when the excited pulse is first created by coalescence. As a result, the speed distribution is narrow, smooth, and skews to the right.

The irreversible and self-sustained coalescence events that produce the large pulses and coarsen the wave texture also increase the average pulse speed and pulse height as seen in Fig. 2. This is because, as the pulse density decreases, the pulses must become bigger to carry the same flow rate. As the pulses get bigger, their substrate layer thickness must also increase to maintain the force balance that sustains the stationary motion of the pulses. There is hence a quasisteady increase in the local normalized Reynolds number Δ , pulse speed D , height H_{\max} , and area A as the average pulse climbs the solitary pulse family in Fig. 5.

The global mass balance that specifies the member of the pulse family at each station can be derived by considering the normalized kinematic condition (5b), which represents a simple mass balance in the moving frame. For a solitary pulse to be steady in the moving frame, the flow rate at every position X , $Q(X) - DH(X)$, must be the same and equal to that of the flat film $1 - D$. Both flow rates are measured in the moving frame which accounts for the terms $-DH$ and D . Because of the localized structure of the pulses, the average over a sequence of randomly spaced pulses with identical speed is equal to that of a periodically spaced pulse train,

$$\langle \dots \rangle = \lim_{X_0 \rightarrow \infty} \frac{1}{X_0} \int_X^{X+X_0} \dots dX = \frac{1}{L} \int_X^{X+L} \dots dX,$$

where L is the average separation. (We shall correct this formulation later to account for the existence of two distinct

pulses.) Applying this averaging to (5b), which is valid for every pulse in a randomly spaced train, and since D is identical for every pulse (or at least has a narrow distribution as seen in Fig. 6) such that $\langle DH \rangle = D \langle H \rangle$, one obtains

$$\langle Q \rangle = D \langle H \rangle + 1 - D = \frac{D}{L} \int_0^L (H - 1) dX + 1 = \frac{DA(\Delta)}{L} + 1, \quad (7)$$

where the last equality applies due to the narrow width of the localized pulse which is much smaller than L . The quantity $\langle Q \rangle$, the space-averaged flow rate, is also the time-averaged flow rate measured at any station as the pulse train passes by. Hence, due to a global mass balance, it must be equal to the time-averaged flow rate at the inlet $\langle q \rangle$ after returning to the original variables of (1). In such variables, $\langle q \rangle = 1$ since the inlet conditions are chosen to scale the variables, and one obtains, after invoking (4),

$$\langle Q \rangle = s^{-3}. \quad (8)$$

Combining this with (7), we obtain the mass balance condition which relates the average separation $\langle l \rangle$ in the original coordinate x to the substrate thickness s of the original scaling and the local normalized Reynolds number,

$$\langle l \rangle = L s^{1/3} = D(\Delta) A(\Delta) s^{10/3} / (1 - s^3). \quad (9a)$$

This estimate neglects the presence of the excited large pulses which will be considered in the next section. Near the inception point of the pulses ($x=200$ in Fig. 1), s is small (see Fig. 2) and (9a) can be further simplified to a relation with a power-law dependence on s :

$$\langle l \rangle \sim D(\Delta) A(\Delta) s^{10/3}. \quad (9b)$$

This power-law scaling and its corrected version will yield generic coarsening exponents near the inception point.

The local normalized Reynolds number Δ is also related to the actual inlet Reynolds number through a power-law scaling in s according to (4):

$$\delta = s^{-11/3} \Delta. \quad (10)$$

Hence, the quasisteady evolution of nearly identical but randomly distributed pulses along the solitary pulse family, their narrow width, and simple mass balance have allowed us to relate the average separation $\langle l \rangle$ at any station to the local average substrate thickness s for a given δ . What remains is to decipher the evolution of $\langle l \rangle$ downstream, and the entire dynamics is known.

Before proceeding to the binary interaction dynamics that determine the evolution of $\langle l \rangle$, we simplify (9) and (10) by noting a certain asymptotic behavior of $D(\Delta)$ and $A(\Delta)$ at relatively large Δ ,

$$\begin{aligned} D(\Delta) &\sim D_\infty = 7.70, \\ A(\Delta) &\sim 23.5\Delta. \end{aligned} \quad (11)$$

It seems that the pulses reach a constant ‘‘terminal velocity’’ at larger Δ and their widths reach a constant, while the area increases linearly with respect to Δ . We are unable to pro-

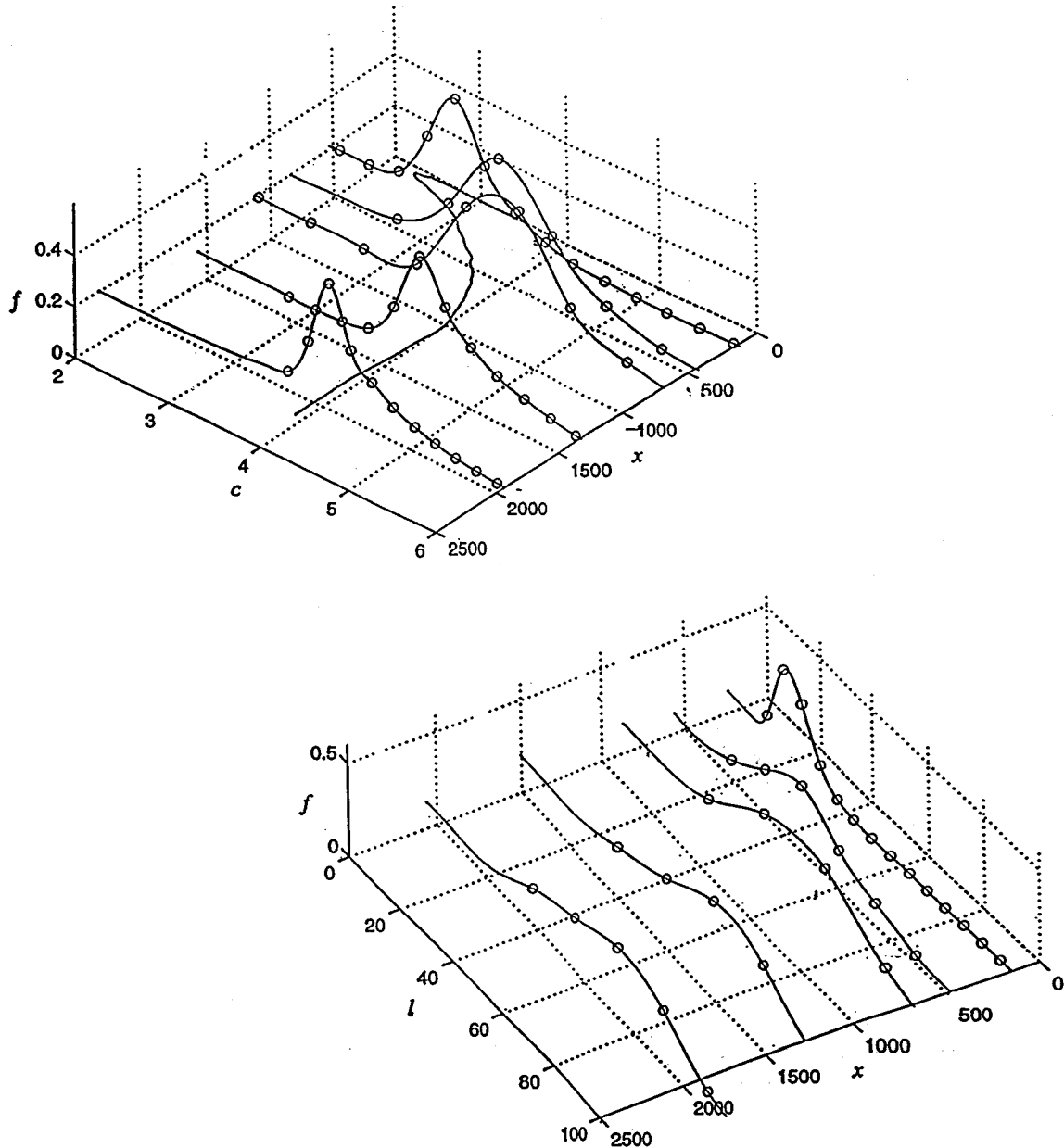


FIG. 6. Pulse speed c and separation distributions at various stations from the simulation of Fig. 1. The downstream evolution of the mean pulse speed in Fig. 2 is also depicted. The speed distribution sharpens dramatically after pulse inception at $x=200$, while the separation distribution broadens. The speed distribution also has a longer tail to the right of its mean.

vide a physical explanation for this large Δ behavior but (11) allows us to simplify the correlation (9b) near the pulse inception point to

$$\langle l \rangle \sim 23.5 D_{\infty} s^7 \delta \quad (12)$$

for relatively large Δ and small s . This provides a more explicit relationship between $\langle l \rangle$ and s for a given inlet Reynolds number δ . More importantly, it retains the power-law affine scalings in s for the average separation $\langle l \rangle$. This will allow us to produce generic exponents common in systems invariant to affine transformation. The range of Δ where (11) is valid also corresponds to most practical conditions for common fluids like water [13].

III. BINARY INTERACTION AND COARSENING DYNAMICS

Much as the average pulse at every station can be normalized to 1 with a unit substrate thickness, the local coalescence rate can also be studied after proper normalization. Such coalescence events correspond to a large pulse chasing down a smaller front pulse. We shall use the smaller pulse as the reference pulse for normalization. We shall also assume that the large pulse has decayed to the extent that it resembles the small pulse at the time of coalescence. Each large pulse is then created from the coalescence of two smaller pulses and is assumed to have twice the area of the latter. Due to its slow decay dynamics, we showed in the earlier report [7] that the large excited pulse is also a member

of the solitary pulse family and exist on a substrate thickness s_e different from s of the small reference pulse. The normalized Reynolds number Δ_e based on s_e is then different from Δ of the small reference pulse. In this model, we hence represent all the pulses at every station by two members of the solitary pulse family at Δ and Δ_e related by

$$2s^{4/3}A(\Delta) = s_e^{4/3}A(\Delta_e). \quad (13)$$

The scaling $s^{4/3}$ results because the true area $a = \int_{-\infty}^{\infty} (h-s)dx$ is related to the normalized area A through (4) by $a = s^{4/3}A$.

Strictly speaking, the area of the large pulse should be equal to the sum of two coalescing pulses upstream. These two pulses may also have different areas if the larger pulse has not decayed sufficiently. Nevertheless, pulses upstream are smaller than the pulses at any given station and we use (13) as a reasonable estimate of the identity of the large pulse at every station. The existence of two distinct pulses is not apparent in the snapshot of Fig. 1 since the large pulses are at different stages of decay. However, the world lines in the same figure clearly show two distinct slopes at every given station. Such world lines capture the pulses over a long interval and are hence more revealing.

Since Δ is also related to s through (10) at a given δ , (13) yields a nonlinear equation,

$$2A(\Delta) = \beta^{4/3}A(\Delta\beta^{11/3}), \quad (14)$$

for $\beta = s_e/s$. Hence, knowing $A(\Delta)$ from Fig. 4 and knowing s , we can determine the substrate thickness beneath the large pulse, s_e , from (14). For the large Δ limit of interest, the linear scaling of $A(\Delta)$ in (11) implies a constant generic ratio close to unity:

$$\beta \approx 2^{1/5}. \quad (15)$$

We shall expand β about 1 in our theory to simplify the analysis.

The fact that β is close to unity also implies that $(\Delta_e/\Delta) = \beta^{11/3} \sim 2^{11/15} \sim 1.66$ and the ratio between two unnormalized pulse speeds, $(c_e/c) = \beta^2$, are both close to unity. The latter explains why the coalescence frequency is lower than the pulse frequency $c/\langle l \rangle$. Since $D(\Delta)$ approaches a constant at large Δ , according to (11) and as seen in Figs. 4 and 5, the closeness of Δ_e to Δ implies that the average speed of the large and small pulses also lies on the $D(\Delta)$ branch of the solitary pulse family, regardless of the fraction of each. This explains why the time-averaged speed still follows the $D(\Delta)$ branch in Fig. 5.

The overall mass balance (9a), however, must be modified to account for the presence of the large pulses,

$$\langle l \rangle = \left[\frac{pA(\Delta_e)s_e^{4/3} + (1-p)A(\Delta)s^{4/3}}{p/c_e + (1-p)/c - ps_e^3/c_e - (1-p)s^3/c} \right], \quad (16a)$$

where p is the fraction of large pulses, $c_e = D(\Delta_e)s_e^2$ is the unnormalized speed of the large pulse, $\Delta_e = \Delta\beta^{11/3} = \Delta(s_e/s)^{11/3}$, and $A_e = A(\Delta_e)$ is the normalized area of the large pulse defined in (13).

For large Δ , (11) and (15) can be used to simplify (16a). Furthermore, if we focus on the region near pulse inception

($x=200$ in Fig. 1), Fig. 2 indicates that s is small in the region and the denominator of (16) can be approximated by $(p/c_e) + (1-p)/c$. If we further carry out an expansion in p , (16a) can be simplified to yield a power-law relationship important for our estimate of the initial coarsening dynamics near inception, which is a correction to (12) for the presence of excited pulses,

$$\langle l \rangle \sim 23.5D_\infty \delta s^7 \frac{1+p}{(p/\beta^2) + 1 - p}. \quad (16b)$$

Condition (14) then identifies the large pulse at every station given the reference small pulse with substrate thickness s . To obtain s from (9a), the evolution of $\langle l \rangle$ must be known; to obtain s from the more accurate (16), however, the evolution of both $\langle l \rangle$ and p downstream must be deciphered. Both require knowledge about how a large pulse chases down a smaller pulse in front to induce coalescence. Such a binary pulse interaction was studied in our earlier paper [7], where we placed a large pulse whose thickness in the normalized coordinate of (4) is $\beta = s_e/s$ behind a reference pulse which exists on a substrate of unit thickness in the normalized coordinate. Due to the difference in the substrate layer thicknesses, mass drains out of the back excited pulse, and its substrate layer thickness β decreases in time according to

$$\frac{d}{dT}(\beta - 1) = -\gamma(\Delta)(\beta - 1), \quad (17)$$

where $T = s^{5/3}t$ is the time coordinate for the normalized problem. The decay coefficient γ was computed in our earlier paper and is plotted in Fig. 4(d). For large Δ values when (11) applies, this decay coefficient can also be approximated by

$$\gamma \sim 0.004\Delta^{-1}, \quad (18)$$

which retains the power-law scaling required for universal exponents.

The separation L between the two pulses decreases at a rate equal to the speed difference between the pulses,

$$\frac{dL}{dT} = -[D(\Delta_e) - D(\Delta)]. \quad (19)$$

Since Δ and s are related through (10), it will be much more convenient to represent both the large pulse speed $D_e = D(\Delta_e) = D(\delta s_e^{11/3})$ and the reference pulse speed $D = D(\Delta) = \Delta(\delta s^{11/3})$ as functions of s_e and s . Equation (19) was derived based on the observation that both the back large excited pulse and the front pulse are quasisteady and hence belong to the solitary pulse family.

Since β is close to unity from our estimate of (15), we can relate D_e to D by a local expansion about $\beta=1$ or $s=s_e$,

$$D_e \sim D + \alpha(s_e - s) \quad (20)$$

or, in the unnormalized form,

$$c_e \sim c + \hat{\alpha}(s_e - s),$$

where

$$\alpha = \left(\frac{\partial D(\delta\chi^{11/3})}{\partial \chi} \right)_{\chi=s}, \quad (21a)$$

$$\hat{\alpha} = \left(\frac{\partial \chi^2 D(\delta\chi^{11/3})}{\partial \chi} \right)_{\chi=s} = \left(\frac{\partial c}{\partial s} \right)_\delta. \quad (21b)$$

This approximation then couples (17) and (19) to yield a simple relationship for how the separation between the two pulses decrease as the decaying large pulse chases down the smaller reference pulse in front,

$$L(T) = L_0 - \frac{\alpha(\beta_0 - 1)s}{\gamma} (1 - e^{\gamma T}),$$

where the subscript 0 denotes the initial values. Hence, the time T_c for coalescence in the normalized coordinate is defined by $L(T_c) = 0$ or

$$T_c = -\frac{1}{\gamma(\Delta)} \ln \left(1 - \frac{\gamma L_0}{\alpha(\beta_0 - 1)s} \right). \quad (22)$$

From (22), an estimate of the equilibrium separation when $T_c = \infty$ (the separation is too large for the back pulse to capture the front one) is immediately available. In the original unnormalized coordinate, it becomes

$$\langle l \rangle_\infty = \frac{\hat{\alpha}(\beta_\infty - 1)}{\gamma(\delta s_\infty^{11/3})s_\infty^{2/3}}. \quad (23)$$

Equation (23), along with (14) and (16), then specifies s_∞ , β_∞ , and $\langle l \rangle_\infty$, the equilibrium substrate thickness, the equilibrium ratio between the substrates of the large and small pulses, and the average separation. There remains an unknown variable p_∞ , corresponding to the fraction of large pulses at equilibrium in (16).

At relatively large Δ values when (11) and (18) hold, simple estimates of the equilibrium values can be obtained by noting $\beta_\infty = \beta = 2^{1/5}$ from (15) and

$$\hat{\alpha} \sim 2sD_\infty \quad (24)$$

while (18) can be used to simplify (23)

$$\begin{aligned} \langle l \rangle_\infty &= \frac{2(\beta - 1)D_\infty s_\infty^{1/3}}{\gamma(\delta s_\infty^{11/3})}, \\ &\sim \frac{D_\infty(\beta - 1)}{0.002} \delta s_\infty^4. \end{aligned}$$

An extra relationship between s_∞ and $\langle l \rangle_\infty$ is provided by (16). Since s is close to unity near equilibrium, as seen in Fig. 2, the more accurate version (16a) must be used. We still invoke the large Δ approximation of (11), which becomes increasingly accurate at large s since Δ increases with s , such that

$$(c_e/c) = (s_e/s)^2 = \beta^2 = 2^{2/5},$$

$$(\Delta_e/\Delta) = \beta^{11/3},$$

to yield

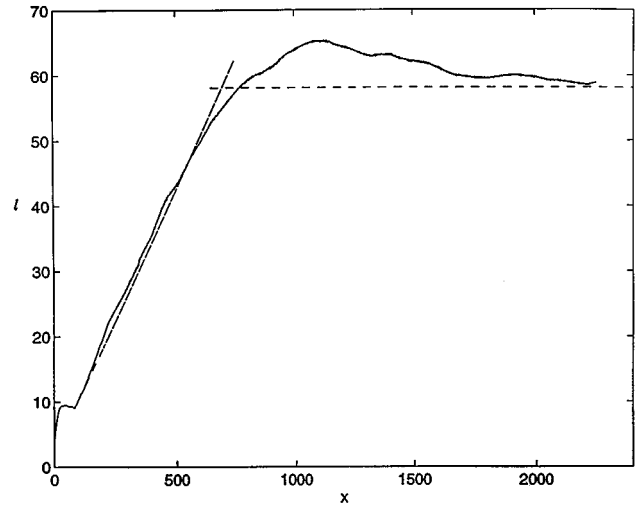


FIG. 7. The coarsening dynamics with downstream separation evolution. The linear initial coarsening rate and the equilibrium separation are well approximated by (35) with $p_0=0.5$ and by (26), respectively.

$$s_\infty = \left[\frac{1 - p_\infty + (p_\infty/\beta^2)}{0.047(1 + p_\infty)/(\beta - 1) + 1 - p_\infty + p_\infty\beta} \right]^{1/3}, \quad (25)$$

$$\langle l \rangle_\infty = D(\beta - 1)\delta s_\infty^4/0.002.$$

As we shall demonstrate, a good estimate for the fraction of excited pulses is 0.5 and it remains relatively constant over a large distance. For this value of p_∞ , we obtain from (25) $s_\infty=0.83$ and $\langle l \rangle_\infty=58$, which are in good agreement with our simulated results of Fig. 2 and Fig. 7, where the simulated $s_\infty=0.80$ and $\langle l \rangle_\infty$ is 60. Since the average wavelength near inception is approximately $2\pi(9\delta)^{-1/2}$ [13] and δ is less than unity for water with $R < 100$, it is clear that $\langle l \rangle_\infty$ is an order of magnitude larger than the average wavelength at inception—there is significant coarsening.

To obtain the linear coarsening rate in Fig. 7, we need to estimate the coalescence rate from the coalescence time T_c in (22). It is convenient for this estimate to define a length scale l_{exp} (where the subscript exp denotes expected value) corresponding to the distance, measured in the laboratory frame, traveled by the large pulse before coalescence. Given an initial separation of l and neglecting the speed differential between the large pulse and the reference pulse in this determination, which is consistent with the estimate (15), we obtain in the original coordinates from (22),

$$l_{\text{exp}} = l - \frac{c}{\gamma s^{5/3}} \ln \left(1 - \frac{\gamma s^{5/3} l}{\hat{\alpha}(\beta - 1)s} \right), \quad (26)$$

where l is the initial separation between the large pulse and the front pulse when the former is first created by the prior coalescence event. Near the inception point of the pulses, the quantity within the logarithm is close to unity and one gets

$$l_{\text{exp}} \sim l \left(1 + \frac{c}{\hat{\alpha}(\beta - 1)s} \right). \quad (27)$$

There is a distribution of separation l with an average equal to $\langle l \rangle$, the average pulse separation. Due to the linear dependence of l , one can simply use $\langle l \rangle$ to describe $\langle l_{\text{exp}} \rangle$,

$$\langle l_{\text{exp}} \rangle = \langle l \rangle \left(1 + \frac{c}{\hat{\alpha}(\beta-1)s} \right). \quad (28)$$

If we now impose the large Δ limit of (11), we obtain

$$\langle l_{\text{exp}} \rangle \sim \langle l \rangle \left(1 + \frac{1}{2(\beta-1)} \right) = \langle l \rangle \left(\frac{2\beta-1}{2(\beta-1)} \right) \sim 4.3 \langle l \rangle. \quad (29)$$

The reason $\langle l_{\text{exp}} \rangle$ scales linearly with respect to $\langle l \rangle$ near pulse inception is because, in this region, the separation is so small that the speed of the large pulse hardly changes during the time it chases down its front neighbor, and the elapsed time for coalescence is simply determined by the difference in the two speeds, $\Delta c = \hat{\alpha}(\beta-1)s$, and the distance traveled, $l[1 + (c/\Delta c)]$, where $(c/\Delta c)$ is only a function of $\beta = 2^{1/5}$ in the large Δ region and is hence constant. The ratio $\langle l_{\text{exp}} \rangle / \langle l \rangle = 4.3$ corresponds to the ratio of coalescence frequency to average wave frequency.

Due to the binary coalescence mechanism, the change in the pulse density $\langle l \rangle^{-1}$ at a particular station over a distance of $\langle l_{\text{exp}} \rangle$ is then the product of the large and small pulse fractions,

$$\frac{1}{\langle l \rangle} \Big|_{x+\langle l_{\text{exp}} \rangle} - \frac{1}{\langle l \rangle} \Big|_x = -\frac{p(1-p)}{\langle l \rangle}, \quad (30)$$

or

$$\frac{d\langle l \rangle}{dx} = \frac{p(1-p)\langle l \rangle}{\langle l_{\text{exp}} \rangle} \quad (31)$$

as a continuum approximation when viewed from a scale much larger than $\langle l_{\text{exp}} \rangle$. From (29), it is then clear that this binary interaction yields a rate

$$\frac{d\langle l \rangle}{dx} \sim \frac{p(1-p)}{4.3}. \quad (32)$$

The coarsening rate (32) will be constant if the fraction of excited pulses p remains constant with respect to x . A model of how p evolves downstream requires some statistical analysis of how the large pulses are distributed among the small reference pulses, viz., their average fractions are inadequate and higher spatial correlation information is necessary. The reason is that when large pulses are arranged in packets separated by packets of reference pulses, the hydraulic jump at the front, which is responsible for the decay dynamics in (17), will only cause the first few large pulses to decay, while the large pulses in the back of the pack remain excited over a distance of $\langle l_{\text{exp}} \rangle$. Exactly how many excited pulses within a packet will decay and become smaller reference pulses over a distance of $\langle l_{\text{exp}} \rangle$ is difficult to estimate. However, we shall show below that p does not vary significantly near pulse inception by this mechanism.

Consider a particular pulse train with M reference pulses and N large pulses while $p = N/(M+N)$ as M and N approach infinity. Arrange the large pulses into K nonempty packets which are separated by at least one reference pulse. We allow for all such possible arrangements, and there are $M!/(M-K)K!$ possible ways of inserting the K packets in M small pulses ($K \leq M, N$) while there are $(N-1)/(N-K)!(K-1)!$ kinds of excited pulse packets. Hence, the number of all possible sequences of M small pulses and N large pulses is $\sum_{K=1}^N (M!/(M-K)K!)[(N-1)/(N-K)!(K-1)!]$ for the case of $M \geq N$. We assume that over $\langle l_{\text{exp}} \rangle$, every boundary small reference pulse leading an excited pulse packet is eliminated due to coalescence, while its back

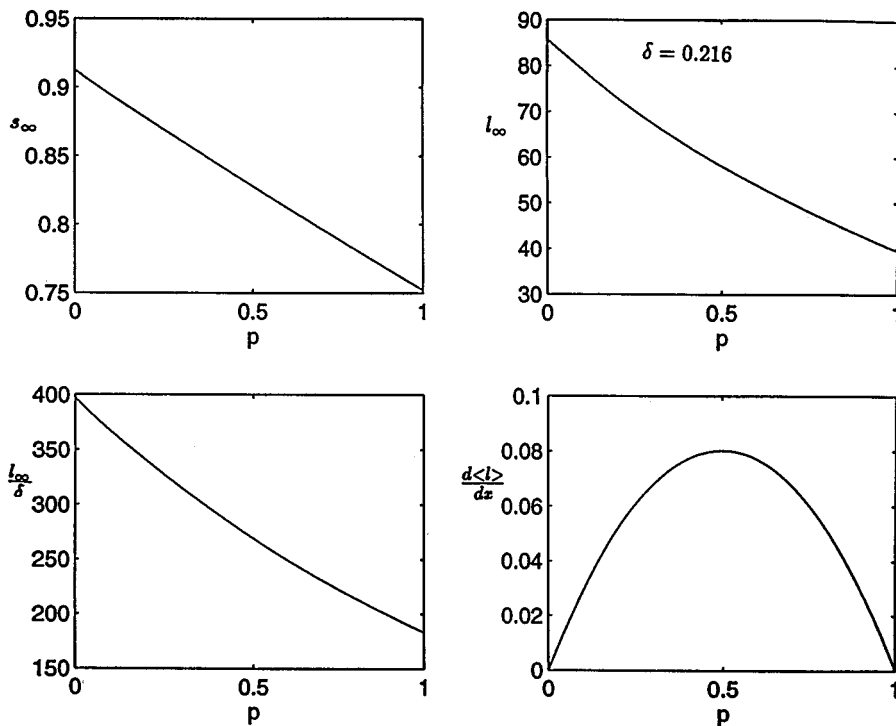


FIG. 8. Dependence of equilibrium substrate thickness, equilibrium separation, and coarsening rate on the fraction p of excited pulses. The equilibrium separation l_∞ scales as δ^{-1} and one of the plots corresponds to the standard case of $\delta=0.216$. The other quantities are independent of δ . Their only dependence on the inlet flow condition and noise is through p_0 , which is also generic at about 0.5 due to the subharmonic secondary instability.

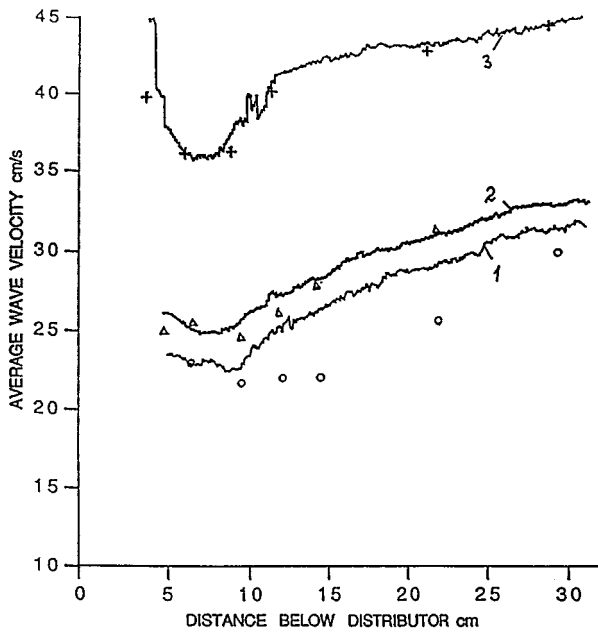


FIG. 9. Simulated downstream evolution of time-averaged speed for (1) $4R=60$, (2) $4R=75$, and (3) $4R=125$ with a white noise amplitude of 5.0×10^{-5} to the unit mean inlet flow rate plotted against Stainthorp and Allen's measured data in circles, triangles, and crosses. The power-law evolution is evident beyond pulse inception at the minimum near 10 cm, corresponding to $x=200$ in Fig. 2.

large neighbor remains a large pulse due to the coalescence. Also, we assume that no other large pulses behind the one participating in the coalescence decay to become smaller reference pulses. The number of reference pulses eliminated by coalescence is then $N - N^2/(M+N)$ in the limit of large M and N . Since the large pulses that participate in the coalescence events remain large pulses over l_{exp} , the change in p is

$$\begin{aligned} \Delta p_0 &= \frac{N}{N + [M - N + N^2/(M+N)]} - \frac{N}{M+N} \\ &= \frac{p^2 - p^3}{1 - p + p^2} \sim p^2, \end{aligned} \quad (33)$$

where the subscript 0 denotes no natural decay of large pulses. Equation (33) is derived for $M \geq N$ but the same result is true for $M < N$.

A simple derivation then yields the following formula for Δp_m when m large pulses behind the leading excited pulse decay to become small reference pulses within $\langle l_{\text{exp}} \rangle$:

$$\Delta p_m = \frac{p^{m+2} - p^3}{1 - p + p^2} \sim O(p^3). \quad (34)$$

The quantity Δp_1 is zero while Δp_0 is positive and $\Delta p_m < 0$ for $m > 1$. The actual Δp is then some weighted average over Δp_m , with the weight decreasing rapidly at large m due to the rare probability of all pulses decaying in a large packet of excited pulses. In addition, since p is less than unity, we see that, regardless of the specific weight, $d\langle l \rangle/dx$ is of $O(p)$ in

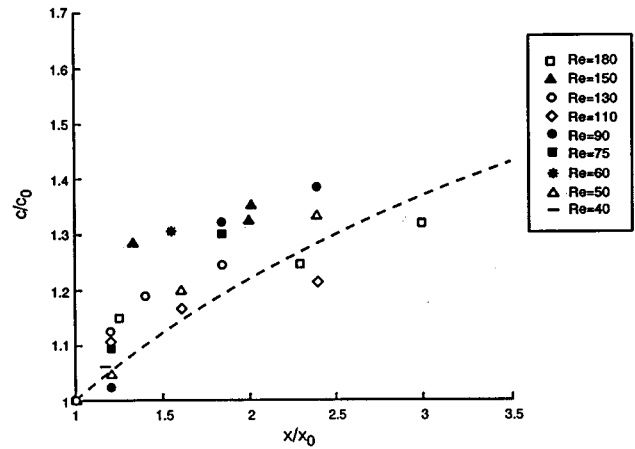
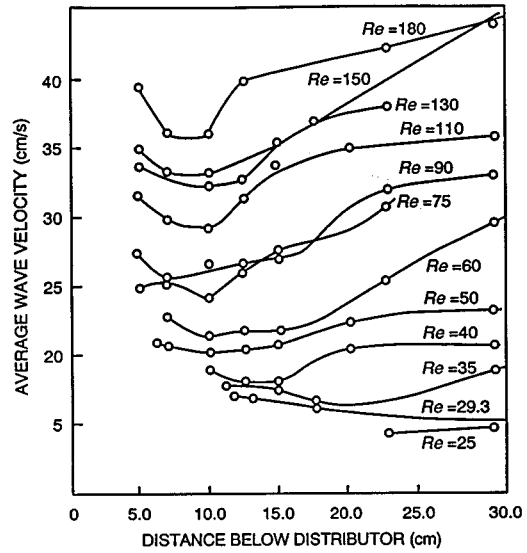


FIG. 10. The raw pulse speed data of Stainthorp and Allen for a vertically falling film. Their Reynolds number Re is related to our R by $Re=4R$. The collapsed data for pulse speeds after inception with $R > 10$ and the dotted curve represent the prediction of (36).

(32) while the variation in p is at most of $O(p^2)$. As a result, over the first few $\langle l_{\text{exp}} \rangle$ (about $10\langle l_{\text{exp}} \rangle$) judging from Fig. 7),

$$\frac{d\langle l \rangle}{dx} \sim p_0(1 - p_0)/4.3 \quad (35)$$

and is a constant dependent only on the initial fraction of large pulses, p_0 .

It remains to determine p_0 , the fraction of large pulses at inception. This fraction is determined by how the pulses are formed from the small-amplitude sinuous waves and is the only part of the pulse dynamics that is determined by inlet noise. Its exact value still escapes us, but it seems to be related to the secondary instabilities of monochromatic waves that precipitate pulse formation for $x < 100$ in Fig. 1 [2,14]. We have shown that the dominant secondary instability is a subharmonic instability with some corruption by a sideband instability [15]. As a result, every other peak in the monochromatic wave field, selected from the broadband inlet noise by a linear filtering mechanism [15], grows rela-

tive to its neighbors when all the peaks are evolving into pulses. As a result, p_0 is close to 0.5 and this yields a slope of 0.08 from (35) compared to the coarsening rate of 0.09 from our simulation in Fig. 7. If we use this value of p in (25) to estimate the equilibrium average substrate thickness and separation, we also obtain reasonable estimates of 0.83 and 58, respectively, which are favorably compared to simulated values in Figs. 2 and 7. Before equilibrium, p will most likely decrease to some unknown value p_∞ due to the natural decay of the excited pulses. However, as seen in Fig. 8, the estimates on s_∞ and $\langle l \rangle_\infty$ do not change appreciably from $p=0.5$ to $p=0.1$.

Finally, the asymptotic behaviors (11) of the solitary pulse speed $D(\Delta)$ and area $A(\Delta)$ yield the near-inception mass balance condition (16b). By combining it with the power-law scaling $c = D_\infty s^2$ and the fact that $d\langle l \rangle/dx$ is constant, for a given δ , the self-similar form

$$\frac{dc}{dx} = \frac{2}{7} \left(\frac{c}{x} \right)$$

is obtained, and hence one has the generic scaling near inception,

$$(c/c_0) \sim (x/x_0)^{2/7}, \quad (36)$$

that the average pulse speed increases as $x^{2/7}$ from its inception point x_0 .

IV. DISCUSSION AND COMPARISON TO EXPERIMENTAL DATA

It is quite surprising that spatio-temporal evolution as complicated as interfacial wave dynamics on a falling film can be described by simple scaling arguments like (25), (35), and (36). The quantities other than $\langle l \rangle_\infty$ depend on the inlet flow conditions and noise only through the fraction of the large pulses, p —they are independent of δ . Even p is found to have a universal constant of 0.5 due to the generic subharmonic instability during pulse inception. The quasisteady

evolution along a normalized solitary pulse family is obviously an important reason which allows the renormalization in the affine transformation (4) in powers of the substrate thickness s . In turn, such power scaling in s is possible because of the scale invariance of the localized solitary pulses which have forgotten the inlet conditions. However, the simple generic exponents are also obtained because the asymptotic behaviors of the solitary pulse family at large Δ in (11) and (18) are power laws in Δ , and because the global mass balance (9) or (16), which is the only way the time-averaged inlet condition is felt at every station, can be approximated by a power-law form at small s near inception. The combination of all these power-law scalings then provides the generic coarsening rate and universal scalings independent of δ and flow conditions.

While Brock [16] has observed a linear increase in the wave separation (period) as in our prediction and simulation, his data are for an inclined film which has an additional parameter—the inclination angle. For vertically falling films, the only available literature data are the average pulse speed measurements of Stainthorp and Allen [17]; and in a recent report [9], we have shown that our numerical simulation can accurately reproduce all their pulse speed data. This required a model of the inlet noise in their experiment, which is assumed to be white noise with an amplitude that is chosen to fit their wave inception data. As seen in Fig. 9, this noise amplitude reproduces their pulse speed evolution accurately at three different values of R for water. The simulated evolution of c does have a power-law increase in x with an exponent close to $2/7$, as predicted. To further confirm this, we have taken all of Stainthorp and Allen's speed data in Fig. 10 and normalized them in the form of (36) to verify the generic $2/7$ power-law speed acceleration. A reasonable collapse of high R data is evident. The theory fails for $R = \text{Re}/4$ below 10 because in this KS limit, the pulses have been shown to be convectively unstable [6].

ACKNOWLEDGMENTS

This work is supported by grants from DOE and NASA.

-
- [1] S. W. Joo and S. H. Davis, *J. Fluid Mech.* **242**, 529 (1992).
 [2] M. Cheng and H.-C. Chang, *Phys. Fluids* **7**, 34 (1995).
 [3] R. J. Deissler, A. Oron, and Y. L. Lee, *Phys. Rev. A* **43**, 4558 (1991).
 [4] T. Kawahara and S. Toh, *Phys. Fluids* **31**, 2103 (1988).
 [5] A. Oron and D. A. Edwards, *Phys. Fluids A* **5**, 506 (1993).
 [6] H.-C. Chang, E. A. Demekhin, and D. I. Kopelevich, *Physica D* **63**, 299 (1993); *Phys. Rev. Lett.* **75**, 1747 (1995).
 [7] H.-C. Chang, E. A. Demekhin, and E. N. Kalaidin, *J. Fluid Mech.* **294**, 123 (1995).
 [8] J. Liu and J. P. Gollub, *Phys. Fluids* **6**, 1702 (1994).
 [9] H.-C. Chang, E. A. Demekhin, and E. N. Kalaidin, *Am. Inst. Chem. Eng. J.* **42**, 1553 (1996).
 [10] V. Ya. Shkadov, *Izv. Akad. Nauk SSSR Mekh. Zhidk. Gaza* **1**, 43 (1967).
 [11] E. A. Demekhin and V. Ya. Shkadov, *Izv. Akad. Nauk SSSR Mekh. Zhidk. Gaza* **3**, 31 (1985).
 [12] P. L. Kapitza and S. P. Kapitza, *Zh. Eksp. Teor. Fiz.* **19**, 105 (1949) [*Sov. Phys. JETP* **19**, 105 (1949)].
 [13] H.-C. Chang, E. A. Demekhin, and D. I. Kopelevich, *J. Fluid Mech.* **250**, 443 (1993).
 [14] J. Liu and J. P. Gollub, *Phys. Rev. Lett.* **70**, 2289 (1993).
 [15] H.-C. Chang, M. Cheng, E. A. Demekhin, and D. I. Kopelevich, *J. Fluid Mech.* **270**, 251 (1994).
 [16] R. R. Brock, *Proc. Am. Soc. Civil Eng. J. Hydraulics Div.* **HY4**, 6704 (1969).
 [17] F. P. Stainthorp and J. M. Allen, *Trans. Inst. Chem. Eng.* **43**, 85 (1965).